Wave attenuation by sea ice in the Arctic marginal ice zone observed by spaceborne SAR

Bing Qing Huang[1,2,3] and Xiao-Ming Li[1,2]

[1] Key Laboratory of Digital Earth Science, Aerospace Information Research Institute, Chinese Academy of Sciences, Beijing, 100094

[2] International Research Center of Big Data for Sustainable Development Goals, Beijing, 100094

[3] University of Chinese Academy of Sciences, Beijing, 100049.

Corresponding author: Xiao-Ming Li (lixm@radi.ac.cn)

Key Points:

- Wave attenuation rate in sea ice was derived based on non-linear inversion of two-dimensional ocean wave spectra by SAR in the Arctic MIZ.
- The attenuation rate generally follows the exponential law, varying with sea state (wave height and period) and sea ice conditions.
- Combining previous studies and this one, we may infer that the wave attenuation in the Artic MIZ is weakening due to sea ice retreat in recent decades.

Abstract

Attenuation of ocean waves by ice is a crucial process of the interaction between waves and sea ice in marginal ice zone (MIZ), while such interaction can contribute to the retreating of sea ice in the Arctic. Based on the retrieved two-dimensional ocean wave spectra by spaceborne SAR, we investigated the attenuation of ocean waves in the MIZ in Svalbard and Greenland. The results show that the energy attenuation rate ranges from $0.126 \times 10^{-4}/m$ to $0.618 \times 10^{-4}/m$. Quantitative analysis suggests that the attenuation rate is significantly related to wave height and peak wave period of coming waves. It is further found that the waves decay faster in the area with ice thickness exceeding 0.5 m. We compared the derived wave attenuation rates in the present study with those in previous studies based on in situ measurements, which reveals that waves are becoming less attenuated by sea ice in the Arctic in recent decades.

Plain Language Summary

The interaction between sea ice and ocean waves is one of the key processes that accelerates the retreat of sea ice in the Arctic. The attenuation of ocean waves by sea ice is crucial to understanding the wave-ice interaction mechanism and predicting ice changes. Spaceborne Synthetic Aperture Radar (SAR), capable of imaging ocean waves and sea ice in two-dimension with high spatial resolution, has shown tremendous potential in studies on wave-ice interaction. In this study, SAR images acquired in ice-covered areas near Svalbard and east of Greenland were collected, and then ocean wave spectra were retrieved from these SAR images. Ocean wave spectra depict sea states elaborately by showing the wave energy distribution in different frequencies and directions. Subsequently, we derived the wave attenuation rate in sea ice from these wave spectra. By comparing the derived attenuation rates with previous field observations, the study reveals a lower attenuation rate, which suggests the waves were less attenuated by ice in past decades under ongoing retreating and thinning of sea ice in the Arctic. This indicates that waves can penetrate sea ice easier and deeper, which may further induce the retreating of sea ice.

1 Introduction

The interaction between sea ice and ocean waves in the Marginal Ice Zone (MIZ) can contribute to the retreat of sea ice in the Arctic (Dumont et al., 2011; Kohout et al., 2014; Thomson & Rogers, 2014). The retreat of sea ice and the northward shifting of MIZ (Jeffries et al., 2013; Rolph et al., 2020; Serreze et al., 2007) increase the ocean fetches, consequently, promoting the growth of ocean waves (Liu et al., 2016; Thomson & Rogers, 2014). The enhanced waves break more sea ice and lead to further melting, with the combined effect of winds and currents. Subsequently, positive feedback is formed and accelerates sea ice retreats (Kohout et al., 2014; Rolph et al., 2020; Thomson & Rogers, 2014). On the other hand, the energy of ocean waves is damped by sea ice. Determination of the wave attenuation rate is key to estimating the ice-breaking extent (Kohout et al., 2014). In addition, the parametrizing of the attenuation process is essential to improving the accuracy of model prediction, in the short and long terms.

Previous studies have shown that attenuation of waves in sea ice is a multifaceted process that can be influenced by incident sea states and ice conditions. Early field experiments carried out in the Bering Sea and the Greenland Sea revealed an exponential decay of wave energy in MIZ, with the attenuation rates ranging from $0.1 \times 10^{-4}/m$ to $8.7 \times 10^{-4}/m$ (Squire & Moore,

1980; Wadhams et al., 1988). Generally, the wave attenuation rate was found to decline with increasing wave period (Squire & Moore, 1980; Wadhams et al., 1988). Recent studies show that the wave energy attenuation rate (α_E) also varies with ice conditions. The two field experiments conducted in the Barents Sea (near Svalbard) show that the α_E derived in 1991 experiment (Frankenstein et al., 2001) was approximately 1.3 times larger than that in 2016 (Tsarau et al., 2017). The significant difference between the two experiments was attributed to changes in ice thickness and floe size. In the Antarctic MIZ, the study by Kohout et al. (2020) shows that strong waves with significant wave height (SWH) greater than 3 m still follow the exponential law along with traveling distance in sea ice, while the attenuation rate is also influenced by wave period and sea ice concentration (SIC).

A massive amount of data is needed to support a comprehensive understanding of attenuation of waves by sea ice, particularly considering the emergence of rapidly changing ice conditions in the Arctic. In-situ observations on a large scale and over a long period can be challenging in the harsh environment of the pole regions. Synthetic Aperture Radar (SAR) has shown significant potential for observing ocean waves in ice-covered areas (Dawe & Parashar, 1978; Lyden et al., 1988; Lyzenga et al., 1985; Raney et al., 1989; Schulz-Stellenfleth et al., 2002; Vachon et al., 1993). Early attempts were made to derive energy attenuation rates in ice based on SAR spectra contrast (Liu et al., 1991; Raney et al., 1989) and they yielded attenuation rates ranging from $0.606 \times 10^{-4}/m$ to $5.7 \times 10^{-4}/m$. However, the method was used under the assumption that imaging of waves by SAR is linear, which, however, often does not hold. The non-linear imaging process of waves by SAR poses challenges in retrieving ocean wave spectrum (OWS) in open water, not to mention in ice-covered areas where the modulation transfer function (MTF) is changed by sea ice (Vachon et al., 1993). An MTF-independent scheme to derive wave height by SAR data was proposed in 1985 (Lyzenga et al., 1985) and was implemented and further developed in recent years (Ardhuin et al., 2015, 2017). With the method, two wave energy attenuation rates were derived, with values of $0.15 \times 10^{-4}/m$ and $0.024 \times 10^{-4}/m$, before and after ice leads, respectively (Stopa et al., 2018). Based on the approach of non-linear retrieval for two-dimensional OWS by SAR in open water (K. Hasselmann & S. Hasselmann,1991, denoted the MPI approach hereafter), a new MTF-based method to retrieve OWS in ice-covered areas was proposed (Huang & Li 2022), referred to MPI-ICE hereafter. By neglecting the hydrodynamic modulation and involving a new tilt modulation in ice in the MTF, the MPI-ICE reduced the squared error of simulated SAR spectra by approximately 50%, compared to the original MPI approach. The progress further facilitates the application of SAR data to quantitative analysis of waves in MIZ. In this study, we aim to derive the attenuation rate of ocean waves propagating in sea ice in the Arctic MIZ based on the retrieved OWS by spaceborne SAR data. Furthermore, the variations in attenuation with different sea states and ice conditions are analyzed in detail.

This paper comprises four sections. Following the introduction, the used data and methods to retrieve OWS by SAR data and to calculate wave attenuation rate are briefly described. Section 3 presents the results based on representative cases. The influences of sea states and ice conditions on wave attenuation were analyzed subsequently. Lastly, we discussed the presented results with the previous observations, and conclusions were drawn.

2 Data and Method

2.1 Data and study area

This study focuses on wave attenuation in the MIZ in Svalbard and Greenland, where the energetic waves strongly interact with sea ice. The used SAR data are the Sentinel-1 (S1) IW (Interferometric Wide Swath) Mode GRDH (Ground Range Detect High resolution) product in Horizontal-Horizontal (HH) polarization. The high spatial resolution (a pixel size of 10 m) and large coverage (a swath of 250 km) of the IW GRDH data provide a clear view of sea ice and ocean waves in the MIZ. In the study area, we collected nine S1 IW images (Figure S1 in the supporting information, SI), presenting clear wave patterns in sea ice in March and April of 2021, when the sea ice achieved the maximum extent of the year. Fourteen transects were selected along the direction of wave propagation to study wave attenuation, with 130 retrieval stations set on them. 82% of the stations were in the area with a thickness within 0.3 m, and 76% were in the compact ice zone with SIC greater than 80%. More details about the selected transects and additional data used for the attenuation study are described in the SI.

2.2 Brief introduction of the MPI-ICE method

Three statistic parameters were used to evaluate the accuracy of the retrieved OWS by SAR using the MPI-ICE method, namely the Converge Index (C.I.), the Correlation between the simulated and observed SAR spectrum (Cor.), and the squared error of the simulated SAR spectrum (Err.). The comparison with the results derived by the MPI approach used in open water shows that the MPI-ICE method reduces the C.I. from 0.83 to 0.54 and decreases the Err. by nearly 50%, suggesting that the proposed MPI-ICE method is more suitable for retrieval of two-dimensional wave spectra in ice-covered areas (Huang & Li, 2022). Using the MPI-ICE method, 130 ocean wave spectra were retrieved in ice-covered areas, and 107 were selected for further wave attenuation study. The selected data are highly accurate, with average C.I., Err., and Cor. of 0.37, 0.25, and 97.41%, respectively. The details of data selection and processing are described in SI.

2.3 Calculation of wave attenuation rate

As pointed out by previous studies, wave energy decays exponentially in ice-covered areas. The energy attenuation rate α_E can be calculated based on equation (1).

$$E = E_0 \exp(-\alpha_E x) \quad (1)$$

Where E and E_0 represent the energy of waves in the ice and the initial energy of waves when entering ice-covered areas, respectively. x is the distance that waves propagate in ice. As the wave energy is proportional to the Hs^2, the wave energy attenuation rate α_E is twice the wave height attenuation rate α_H. The latter can be derived by fitting the linear relationship between $ln(Hs)$ and x:

$$lnHs = -\alpha_H x + b \quad (2)$$

The constant b is introduced to represent the $ln(Hs_0)$, as a reliable Hs_0 in the ice edge is difficult to determine, where the ice is highly mixed with open water. The inhomogeneous characteristics of SAR images pose challenges in retrievals. With the derivation of α_H by fitting, the α_E is derived subsequently.

The fitting process is sensitive to data fluctuations, especially in transects with limited reasonable retrievals. Therefore, a method of seeking a median was employed to determine the α_H as a supplement. Based on Equations (3) and (2), the set of α_H can be calculated. The SWH retrieved at station i and its preceding station j are represented as $Hs(i)$ and $Hs(j)$. dx represents the distance between stations i and j. In instances where the available retrievals along the transect are less than five, the other transects with comparable incident sea states and ice conditions were gathered to calculate a set A. The α_H is determined subsequently by seeking the median. For the transects with a data volume larger than six, the α_H determined by median seeking is used as a referee.

$$A = \{\alpha_{21}, \alpha_{31}, \alpha_{32} \dots \dots \alpha_{ij}, \dots \dots, \alpha_{NN-1}\}\ 2 \le i \le N, 1 \le j < \mathrm{i} \quad (3)$$

$$\alpha_{ij} = -\frac{dln(Hs)}{dx} = -\frac{ln(Hs(i)) - ln(Hs(j))}{dx} \quad (2)$$

3 Results

The α_E derived in this study ranges from $0.126\times 10^{-4}/m$ to $0.618 \times 10^{-4}/m$ and varies with ice conditions and sea states. Details of each transect are shown in Table S1. In the cases selected near Svalbard, where the new ice and young ice with a thickness smaller than 0.3 m predominated, the waves entered with peak wave period (PWP) shorter than 12 s and initial SWH ranges from 0.52 m to 2.15 m. The calculated α_E ranges from $0.198\times 10^{-4}/m$ to $0.618\times 10^{-4}/m$. In the cases east of Greenland, in addition to the dominated young ice and thin first-year ice, thick first-year ice and old ice with thickness exceeding 0.5 m existed in the inner of selected transects. Waves entered the Greenland ice-covered areas with PWP over 13 s and an initial SWH of approximately 2 m. The α_E ranges from 0.126 to $0.270 \times 10^{-4}/m$, generally lower than those achieved near Svalbard ($0.198\sim 0.618\times 10^{-4}/m$). Two cases in Svalbard and Greenland are presented in the following for detailed analysis.

3.1 Wave attenuation of representative cases

The first case presented is that ocean waves propagated in the Svalbard MIZ on March 21, 2021. Figure 1 (a) displays the S1 IW image and the enlarged view of a sub-image showing clear wave patterns in ice-covered areas. The two transects 0321-T1 and 0321-T2 were selected from the ice edge to the edge of the S1 image along the propagation direction of the southeastward wave, spanning the distance of 28 km and 97 km, respectively. Figure 1 (b) shows the SMOS (Soil Moisture and Ocean Salinity)/SMAP (Soil Moisture Active Passive) combined sea ice thickness (SIT) of the day. The ice thickness along both transects was less than 0.3 m. The ERA5 (European Center for Medium-Range Weather Forecasts Reanalysis v5) wave product (the contours and arrows in Figure 1 (b)) shows the incident waves had SWH of 1.9 m and propagated southeastward.

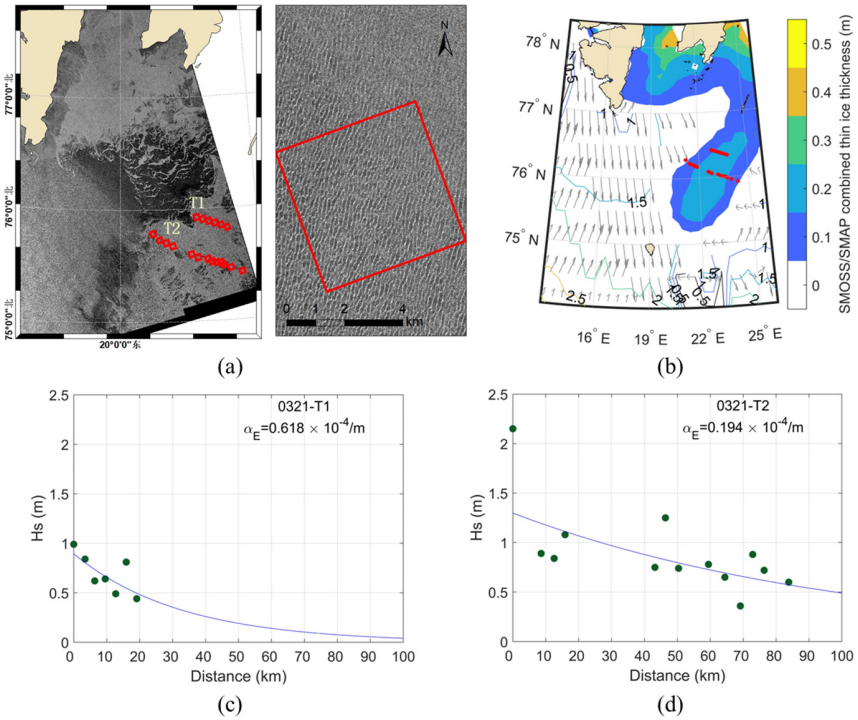

Figure 1. The case on March 21, 2021, in Svalbard: (a) shows the S1 IW image acquired covering part of Svalbard (the northern part of the image). The red squares in the two transects represent the sub-images selected for retrievals of OWS. The enlarged view of a sub-image in transect 0321-T2 is shown in the right panel. (b) is the corresponding map of thin ice thickness. The red dots in the image represent the locations of sub-images. The contours and gray arrows show the SWH and mean wave direction of the most energetic wave system in this region. (c) and (d) show the attenuation of SWH along the transects 0321-T1 and 0321-T2, with the blue lines representing the fitted line based on the exponential model.

The changes of SWH along the transects 0321-T1 and 0321-T2 are shown in Figure 2(c) and (d). The α_E in 0321-T1 is $0.618 \times 10^{-4}/m$, which is much higher than that $(0.194 \times 10^{-4}/m)$ in transect 0321-T2. The difference can be partially attributed to the initial SWH (0.99 m vs. 2.15 m), while the ice condition (new ice and young ice) and initial PWP (~ 10 s) along the two transects were nearly identical. Although the two transects are only approximately 30 km away, the major discrepancy of initial SWH is caused by the shadow effect of Svalbard. Moreover, sea ice also covers a partial region in the northwest of transect 0321-T1, and the fetch is significantly reduced for the growth of waves as the wind blows from the northwest (inferred from the ERA-5 wave data).

错误!未找到引用源。 shows the case east of the Greenland Sea on April 6, 2021. Figure 2 错误!未找到引用源。 (a) is the S1 IW image and the enlarged view of a sub-image in 0406-T4, presenting clear wave patterns. From the ice edge to where wave patterns vanished (visual inspection), transects 0406-T1, T2, and T3 were selected with lengths of 33 km, 57 km, and 46 km, respectively. As the map of sea ice thickness in Figure 2 (b) reveals, the three transects were located partially in the area where ice thickness exceeded 0.5 m. Especially the transect 0406-T1, as shown from the map of ice type on April 8 (Figure 2 (c), based on the U.S.

National Ice Center Arctic Sea Ice Charts and Climatologies in Gridded Format product, referred to NIC ice chart hereafter), the transect located in the area dominated by thick first-year ice and old ice with the typical ice thickness exceeded 1.2 m (WMO, 2010). Transects 0406-T4 and 0406-T5 were chosen near the ice edge, where the ice thickness was less than 0.4 m. The waves propagated over 80 km along transects T4 and T5 before entering the open sea again.

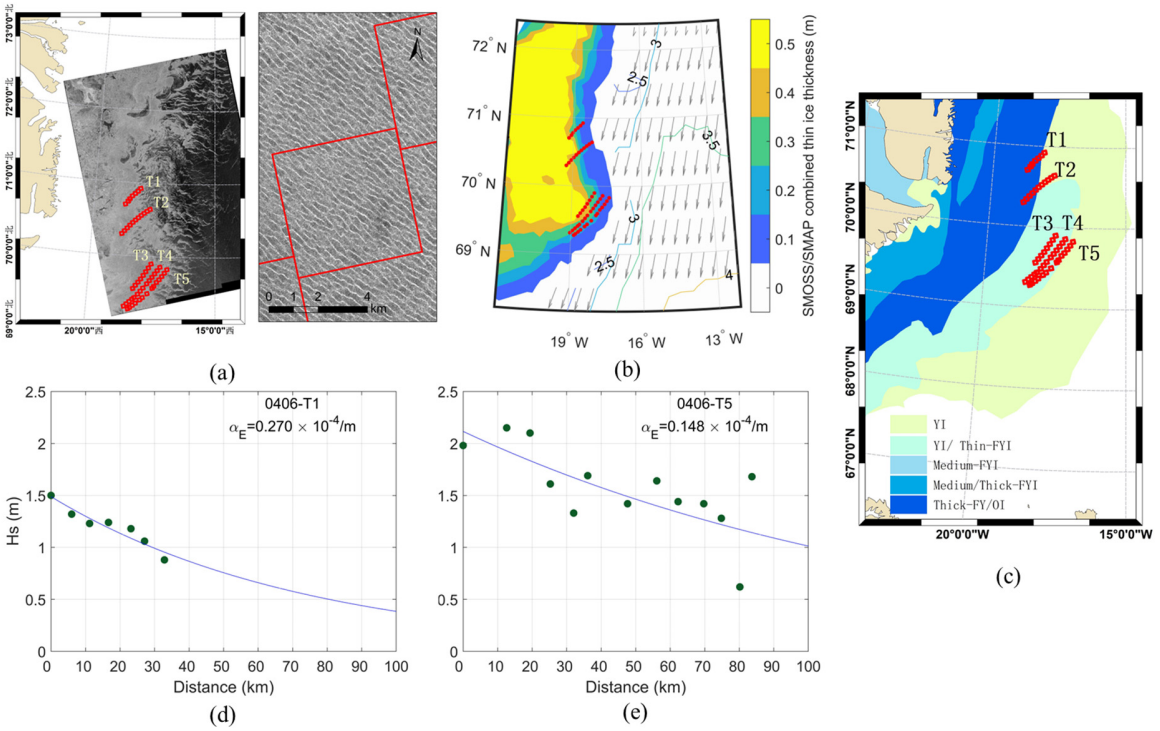

Figure 2. (a) S1 IW images acquired on April 6, 2021, in the east of the Greenland Sea, and the enlarged view of the sub-image is shown in the right panel. The red squares represent the sub-images selected for retrieval. (b) is the corresponding map of the SMOS/SMAP SIT. The red dots represent the sub-image locations. (c) shows the map of ice type based on the NIC ice chart product on April 8. (d) and (e) show SWH changes along the transects 0406-T1 and 0406-T5, respectively, with the blue line representing the fitted line.

Here only the variations of SWH in transect 0406-T1 and T5 are presented in Figure 2 (d) and (e), respectively. Along the transect 0406-T1, the waves were attenuated faster than those in 0406-T5, with an energy attenuation rate of $0.270 \times 10^{-4}/m$ vs. $0.148 \times 10^{-4}/m$. Besides, the wave patterns in SAR images can reveal that the waves were attenuated with different rates in the two transects. In 0406-T1, wave patterns are invisible in the S1 image after propagating approximately 50 km in the ice-covered area, whereas the waves in 0406-T5 propagated over 80 km before entering the open water again. The difference is considered to be attributed to ice conditions. As shown in Figure 2 (c), the inner parts of transects 0406-T1 were occupied by thick first-year ice and old ice. Therefore, it is inferred that the SIT in 0406-T1 should be much thicker than that in 0406-T5 (where the young ice and thin first-year ice with a thickness within 0.4 m dominated). The discrepancy in ice thickness may explain why the α_E in 0406-T1 is approximately two times higher than that in 0406-T5, while their initial SWH and PWP are comparable.

In addition to the influence of initial SWH on wave attenuation rate, the influence of incident PWP is demonstrated through the comparison between the two presented cases in transect 0321-T2 (Figure 1(d)) and 0406-T5 (Figure 2 (e)). Both transects were selected in the area with ice thickness smaller than 0.4 m, and the initial SWHs are approximately 2 m. However, the PWP of waves in 0406-T5 was longer (13.11 s) than that (10.08 s) of 0321-T2. Consequently, the waves in 0406-T5 attenuated with a smaller α_E of $0.148 \times 10^{-4}/m$, compared with the α_E in 0321-T2 of $0.194 \times 10^{-4}/m$.

3.2 Variation of wave attenuation with sea state

To gain further insight into the characteristics of attenuation rates, the retrieved results were divided into three groups based on the initial SWH (represented as H_s) and PWP (represented as T_p), as displayed in Figure 3. The results show that the waves with $H_s \leq 1\ m$ and $10 \leq T_p \leq 12\ s$ exhibit the largest α_E, with a value of $0.448 \times 10^{-4}/m$. For waves with $H_s > 1\ m$ and $10 \leq T_p \leq 14\ s$, the attenuation rate has some fluctuations, as demonstrated in Figure 3 (b) and (c). In Figure 3 (b), the α_E of $0.172 \times 10^{-4}/m$ is achieved for waves with higher SWH ($H_s > 1\ m$) yet still with $10 \leq T_p \leq 12\ s$. For (c), the α_E of $0.0153 \times 10^{-4}/m$ is achieved under the condition that waves with initial SWH greater than 1 m (but not higher than 2.15 m) and $T_p \geq 13\ s$ (but no longer than 14 s).

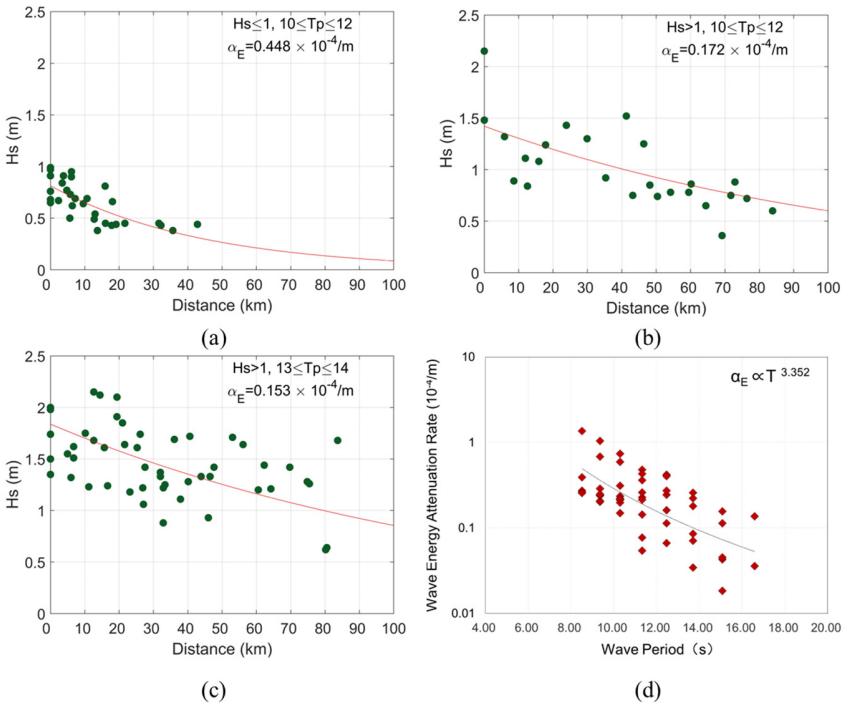

Figure 3. Wave attenuation rates under various sea states: (a) $H_s \leq 1\ m$ and $10 \leq T_p \leq 12\ s$; (b) $H_s > 1$ m and $10 \leq T_p \leq 12\ s$; (c) $H_s > 1$ m and $13 \leq T_p \leq 14\ s$. (d) shows the attenuation rate changes with the wave period.

By Integrating all the S1-retrieved ocean wave spectra along the directions, the frequency spectra were derived, and then the energy attenuation rate at each frequency bin was calculated.

As illustrated by Figure 3 (d), the wave energy attenuation rate declines with the increasing wave period. It is inversely proportional to $T^{3.4}$.

4 Discussion and conclusion

We compared the SAR-derived wave energy attenuation rate in this study with those achieved in previous studies based on in situ measurements, as illustrated in Figure 4.

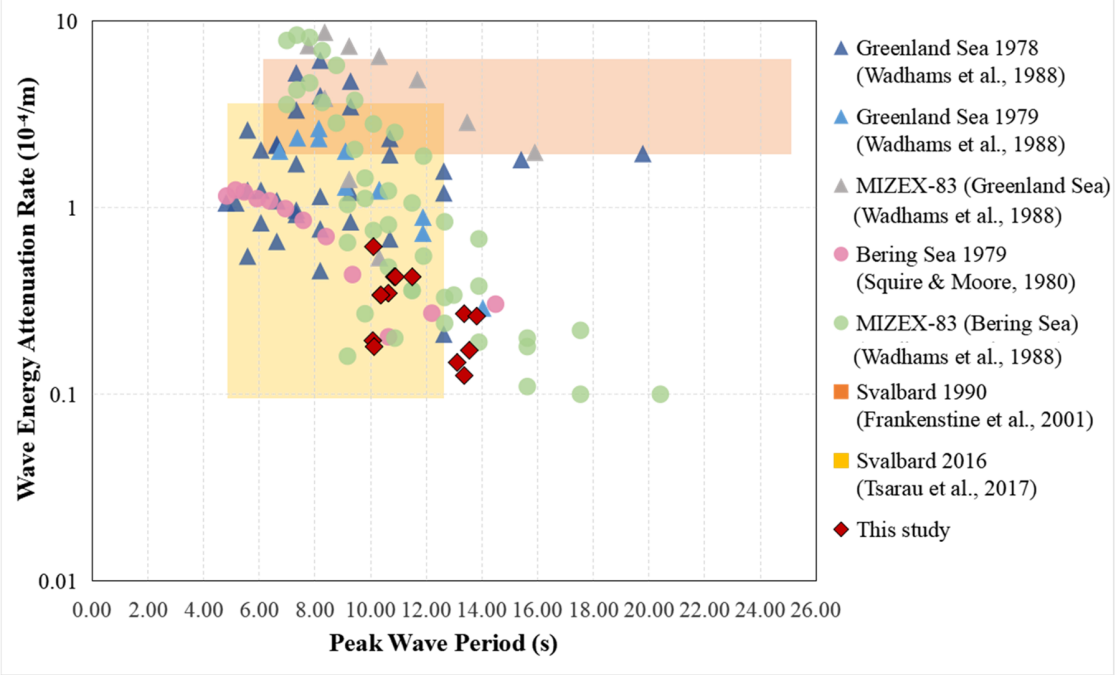

Figure 4. Comparison of the wave attenuation rate in the present study (red diamonds) with those achieved in previous studies in the Artic MIZ.

The α_E achieved in the Greenland Sea in the Marginal Ice Zone Experiment (MIZEX) and earlier field experiments (Wadhams et al., 1988) are depicted in Figure 4, with navy blue, blue, and gray rectangles representing the results derived based on the experiments in 1978, 1979, and 1983, respectively. The α_E derived in the east of Greenland has a range of $0.21\sim8.72 \times 10^{-4}/m$, with 91% of results exceeding $0.618 \times 10^{-4}/m$ (the maximum value of wave attenuation rate derived in this study). We noticed that the multiyear ice with an average thickness of 3.1 m existed during the experimental period in the Greenland Sea (Wadhams et al., 1988). However, the study area of this paper was primarily dominated by new ice, young ice, and thin first-year ice. As thick ice is known to damp wave energy more effectively than thin ice (Robin 1963; Rogers et al., 2021), it is no surprise that a higher α_E was found in the early observations. In contrast, thin and small floes dominated the Bering Sea during the MIZEX (Wadhams et al., 1988) and early field experiments (Squire & Moore, 1980), similar to the ice conditions in this study. The α_E derived in the Bering Sea experiments ranges from $0.1 \times 10^{-4}/m$ to $8.41 \times 10^{-4}/m$ with 55% results lower than $1 \times 10^{-4}/m$, which is comparable to the results derived in this study ($0.126\sim0.618 \times 10^{-4}/m$). However, the short waves with peak periods shorter than 10 s were observed in the Bering Sea field experiments, while the wave period in this study ranges from 10 s to 14 s. Correspondingly, the attenuation rates derived in this study have a lower up boundary than those observed in the Bering Sea field experiment. Additionally, the thickness of sea ice in the Bering Sea ranged from 0.4 m to 1.2 m,

which is thicker than those in this study (with an average of 0.2 m). The thick ice also contributed to the higher attenuation rates derived from the Bering Sea experiments.

The yellow and orange blocks represent the α_E ranges derived in the experiments conducted near Svalbard in the spring of 1990 (Frankenstein et al., 2001) and 2016 (Tsarau et al., 2017), respectively. We noticed an interesting phenomenon that the wave attenuation rates achieved near Svalbard show a declining trend. In the experiment Svalbard 1991, the area was predominated by ice with an average thickness of 1.3 m and a SIC of nearly 100%. The derived α_E ranges from $2 \times 10^{-4}/m$ to $6 \times 10^{-4}/m$, which is generally higher than those derived in the experiment Svalbard 2016 ($0.1{\sim}3.5 \times 10^{-4}/m$). In our study, the attenuation rates in the Svalbard cases are in the range of $0.126{\sim}0.618\times 10^{-4}/m$, which is near the low boundary of Svalbard 2016 ($0.1\times 10^{-4}/m$). The ice conditions in this study (average thickness of 0.2 m) are similar to that in 2016 (with an average of 0.3 m) and show a significant decline in ice thickness since the 1990 experiment. Waves were less damped by thin ice and yielded smaller α_E correspondingly.

The α_E achieved in the Svalbard 2016 experiment has a high-up boundary ($3.5\times 10^{-4}/m$), which corresponds to the waves with a period ranging from 5 s to 10 s. However, the wave period in this study ranged from 10 s to 14 s and the analysis in the previous subsection suggests that waves with longer periods have lower attenuation rates than those with short periods. Therefore, the corresponding α_E in this study is generally lower than those achieved in the 2016 experiment. Within the same period range, i.e., 10~12.5 s, the attenuation rates derived in the 2016 experiment were approximately $0.1 \times 10^{-4}/m$, which is lower than those derived in this study ($0.180{\sim}0.618\times 10^{-4}/m$). We noticed that the waves observed in the Svalbard 2016 experiment entered ice-covered areas with SWH up to 3 m. However, the incident waves carried less energy in this study, with the largest initial SWH of 2.15 m, and therefore, they are easier damped by sea ice and result in higher attenuation rates.

In this study, based on SAR-derived two-dimensional OWS in ice-covered areas, we analyzed wave attenuation in the MIZ in Svalbard and Greenland through a few cases. The attenuation rate of wave energy follows the exponential law against traveling distance, consistent with previous studies conducted in the Arctic. This also suggests the reliability of the MPI-ICE retrievals based on SAR observations to derive ocean wave attenuations, compared with previous studies using in situ buoy observations.

The analysis illustrates that the attenuation of waves in ice is a complex process vulnerable to sea states and ice conditions. Among the cases, the largest α_E is achieved for SWH lower than 1 m and PWP shorter than 12 s. The higher waves with longer periods (swells) generally decay slower. For waves in ice-covered areas with thickness exceeding 0.5 m, the α_E is approximately 2 times higher than that derived in thin-ice areas. Although the attenuation of waves in sea ice is governed by a few factors of sea state and sea ice conditions, the changing trend of the wave attenuation in Svalbard may reflect a reality that the ocean waves are less attenuated by sea ice in the Arctic MIZ in recent decades. The dramatic change of sea ice emerging in the Arctic triggers more complicated wave-ice interaction than ever. We need to collect extensive data on various sea states and ice conditions for a comprehensive understanding of such interactions and their feedback on ice retreats.

Acknowledgments

We thank the European Space Agency for providing the Sentinel-1 data, and the National Marine Environment Forecasting Center for providing the WW3 model data. The ERA5 reanalysis data were downloaded from https://cds.climate.copernicus.eu/cdsapp#!/dataset/reanalysis-era5-single-levels-monthly-means?tab=form. The SMOS and SMAP combined thickness of thin ice product, as well as the AMSR-2 sea ice concentration product, were downloaded from https://seaice.uni-bremen.de/data/. The U.S. National Ice Center Arctic and Antarctic Sea Ice Charts were downloaded from https://nsidc.org/data/g10013/versions/1. The study was supported by the National Science Fund for Distinguished Young Scholars (42025605).

References

Ardhuin, F., Collard, F., Chapron, B., Girard-Ardhuin, F., Guitton, G., Mouche, A., et al. (2015). Estimates of ocean wave heights and attenuation in sea ice using the SAR wave mode on Sentinel-1A. *Geophysical Research Letters*, 42, 2317-2325. https://doi.org/10.1002/2014GL062940

Ardhuin, F., Stopa, J., Chapron, B., Collard, F., Smith, M., Thomson, J., et al. (2017). Measuring ocean waves in sea ice using SAR imagery: A quasi-deterministic approach evaluated with Sentinel-1 and in situ data. *Remote Sensing of Environment*, 189, 211-222. http://dx.doi.org/10.1016/j.rse.2016.11.024

Dawe, B., & Parashar, S. (1978). *SAR Imaging of waves in ice*. Paper presented at Oceans '78, Washington, DC. https://doi.org/10.1109/OCEANS.1978.1151122

Dumont, D., Kohout, A.L., & Bertino, L. (2011). A wave-based model for the marginal ice zone including a floe breaking parameterization. *Journal of Geophysical Research Oceans,* 116(C4), 1-10. https://doi.org/10.1029/2010JC006682

Fernand, M. (1994). Topographic distance and watershed lines. *Signal Processing*, 38, 113-125. https://doi.org/10.1016/0165-1684(94)90060-4

Frankenstein, S., Løset, S., & Shen, H.H. (2001). Wave–ice interactions in Barents Sea marginal ice zone. *Journal of Cold Regions Engineering*, 15 (2), 91–102. https://doi.org/10.1061/(asce)0887-381x(2001)15:2(91)

Hasselmann, K., & Hasselmann, S. (1991). On the nonlinear mapping of an ocean wave spectrum into a synthetic aperture radar image spectrum and its inversion. *Journal of Geophysical Research Oceans*, 96(C6), 10713-10729. https://doi.org/10.1029/91JC00302

Huang, B. & Li, X-M. (2022). Study on retrievals of ocean wave spectrum by spaceborne SAR in ice-covered areas. *Remote Sensing*. 2022, 14(23), 6086. https://doi.org/10.3390/rs14236086

Jeffries, M.O., Overland, J.E., & Perovich, D.K. (2013). The Arctic shifts to a new normal. *Physics Today*, 66 (10), 35. https://doi.org/10.1063/PT.3.2147

Kohout, A.L., Williams, M.J.M., Dean, S.M., & Meylan, M.H. (2014). Storm-induced sea-ice breakup and the implications for ice extent. *Nature*, 509, 604-607. https://doi.org/10.1038/nature13262

Kohout, A. L., Smith, M., Roach, L. A., Williams, G., Montiel, F., & Williams, M. J. M. (2020). Observations of exponential wave attenuation in Antarctic sea ice during the PIPERS campaign. *Annals of Glaciology*, 61(82), 196-209. https://doi.org/10.1017/aog.2020.36

Liu, A.K., Holt, B., & Vachon, P.W. (1991). Wave propagation in the marginal ice zone: Model predictions and comparisons with buoy and synthetic aperture radar data. *Journal of Geophysical Research Oceans*, 96(C3), 4605-4621. https://doi.org/10.1029/90JC02267

Liu, Q., Babanin, A.V., Zieger, S., Young, I.R., & Guan, C. (2016). Wind and wave climate in the Arctic Ocean as observed by altimeters. *Journal of Climate*, 29(22), 7957-7957. https://doi.org/10.1175/JCLI-D-16-0219.1

Lyden, J., Schuchman, R., Zago, C., Rottier, R, Wadhams, P., & Jahannessen, O. (1988). SAR imaging of ocean waves in the Marginal Ice Zone. *IEEE Geoscience and Remote Sensing Symposium 1988*, IEEE, Edinburgh, Scotland. https://doi.org/10.1109/IGARSS.1988.569488

Lyzenga, D.R., Shuchman, R.A., & Lyden, J.D. (1985). SAR imaging of waves in water and ice: Evidence for velocity bunching. *Journal of Geophysical Research Oceans*, 90(C1), 1031-1036. https://doi.org/10.1029/JC090iC01p01031

Raney, R.K., Vachon, P.W., De Abreuet, R.A., & Bhogal, A.S. (1989). Airborne SAR observations of ocean surface waves penetrating floating ice. *IEEE Transactions on Geoscience and Remote Sensing 1989*, 27(5), 492-500. https://doi.org/10.1109/TGRS.1989.35932

Robin, G.Q. (1963). Wave propagation through fields of pack ice. *Philosophical Transactions of the Royal Society of London*, 255(1057),313-339. https://doi.org/10.1098/rsta.1963.0006

Rogers, W.E., Meylan, M.H., & Kohout., A.L. (2021). Estimates of spectral wave attenuation in Antarctic sea ice, using model/data inversion. *Cold Regions Science and Technology*, 182,1-13. https://doi.org/10.1016/j.coldregions.2020.103198

Rolph, R.J., Feltham, D.L., & Schröder, D. (2020). Changes of the Arctic marginal ice zone during the satellite era. *The Cryosphere*, 14(6), 1971-1984. https://doi.org/10.5194/tc-14-1971-2020

Schulz-Stellenfleth, J., & Lehner, S. (2002). Spaceborne synthetic aperture radar observations of ocean waves traveling into sea ice. *Journal of Geophysical Research Oceans*, 107(C8), 20-1-20-19. https://doi.org/10.1029/2001JC000837

Serreze, M. C., Holland, M. M., & Stroeve J. (2007). Perspectives on the arctic's shrinking sea-ice cover. *Science*, 315(5818), 1533-1536. https://doi.org/10.1126/science.1139426

Squire, V. A., & Moore, S. C. (1980). Direct measurement of the attenuation of ocean waves by pack ice. *Nature*, 283, 365–368. https://doi.org/10.1038/283365a0

Stopa, J. E., Ardhuin, F., Thomson, J., Smith, M.M., Kohout, A.L., Doble, M., & Wadhams, P. (2018). Wave attenuation through an Arctic marginal ice zone on 12 October 2015: 1. Measurement of wave spectra and ice features from Sentinel 1A. *Journal of Geophysical Research: Oceans,* 123(5), 3619-3634. https://doi.org/10.1029/2018JC013791

The WAVEWATCH III Development Group (WW3DG). (2019). User manual and system documentation of WAVEWATCH III version 6.07. Maryland, USA, NOAA/NWS/NCEP/MMAB.

Thomson, J., & Rogers W. E. (2014). Swell and sea in the emerging Arctic Ocean. *Geophysical Research Letter*, 41, 3136–3140. doi:10.1002/2014GL059983.

Tsarau, A., Shestov, A., & Løset, S. (2017). *Wave attenuation in the Barents Sea marginal ice zone in the spring of 2016*. The 24th International Conference on Port and Ocean Engineering under Arctic Conditions, Busan, South Korea

Vachon, P.W., Olsen, R., Krogstad, H.E., & Liu, A.K. (1993). Airborne synthetic aperture radar observations and simulations for waves in ice. *Journal of Geophysical Research*, 98(C9)，16411-16425. https://doi.org/10.1029/93JC00914

Wadhams, P., Squire, V. A., Goodman, D. J., Cowan, A.M., & Moore, S.C. (1988). The attenuation rates of ocean waves in the marginal ice zone. *Journal of Geophysical Research*, 93(C6), 6799-6818. https://doi.org/10.1029/JC093iC06p06799

World Meteorological Organization (WMO). (2010). SIGRID-3: A vector archive format for sea ice charts. Intergovernmental Oceanographic Commission. https://library.wmo.int/index.php?lvl=notice_display&id=11295#.Yh1CrSxlCqR